

High-Fidelity, Customizable Force Sensing for the Wearable Human-Robot Interface

Noah Rubin¹, Ava Schraeder^{2,*}, Hrishikesh Sahu^{2,*}, Thomas C. Bulea¹, and Lillian Chin²

Abstract— Mechanically characterizing the human-machine interface is essential to understanding user behavior and optimizing wearable robot performance. This interface has been challenging to sensorize due to manufacturing complexity and non-linear sensor responses. Here, we measure human limb-device interaction via fluidic innervation, creating a 3D-printed silicone pad with embedded air channels to measure forces. As forces are applied to the pad, the air channels compress, resulting in a pressure change measurable by off-the-shelf pressure transducers. We demonstrate in benchtop testing that pad pressure is highly linearly related to applied force ($R^2 = 0.998$). This is confirmed with clinical dynamometer correlations with isometric knee torque, where above-knee pressure was highly correlated with flexion torque ($R^2 = 0.95$), while below-knee pressure was highly correlated with extension torque ($R^2 = 0.75$). We build on these idealized settings to test pad performance in more unconstrained settings. We place the pad over *biceps brachii* during cyclic curls and stepwise isometric holds, observing a correlation between pressure and elbow angle. Finally, we integrated the sensor into the strap of a lower-extremity robotic exoskeleton and recorded pad pressure during repeated squats with the device unpowered. Pad pressure tracked squat phase and overall task dynamics consistently. Overall, our preliminary results suggest fluidic innervation is a readily customizable sensing modality with high signal-to-noise ratio and temporal resolution for capturing human-machine mechanical interaction. In the long-term, this modality may provide an alternative real-time sensing input to control / optimize wearable robotic systems and to capture user function during device use.

I. INTRODUCTION

Wearable robotic devices are becoming increasingly popular as a method to enhance and measure human movement. Traditionally, “wearable robotics” has been synonymous with exoskeletons that exert a force on the human body to assist and/or rehabilitate movement [1]. With the rise of soft robotics, the term expanded to include haptic interfaces, compression therapies, and dynamically-changing fashion [2]. A fundamental design challenge persists across these many different wearable robotic applications: what should the mechanical interface between human and machine look like? This interface is defined by the forces and torques applied by the human against their device (and vice versa). Thus, mechanically characterizing the human-device interaction can provide useful information, such as movement intent and force output, as well as providing insight into fundamental aspects of user motor control and even pathophysiology [3].

*These authors contributed equally to this work.

¹Rehabilitation Medicine Department, National Institutes of Health (NIH) Clinical Center, Bethesda, Maryland, USA.

²Department of Electrical and Computer Engineering, University of Texas at Austin, Austin, Texas, USA.

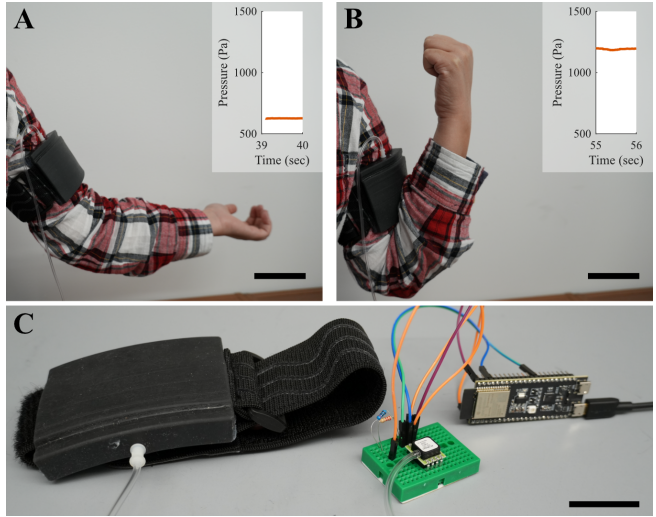


Fig. 1. Demonstration of a person wearing the sensorized pad at (A) rest and (B) full elbow flexion. The insets show representative data of the reported pad pressure. (C) Overview of the sensorized pad system. From left to right, the black fluidically innervated pad on a strap. The pad is connected by a white barb and transparent silicone tubing to an off-the-shelf pressure transducer on a green breadboard. The transducer connects to an ESP-32 microcontroller which streams the data to the main computer. All scale bars are 5 cm

Despite this importance, the human-machine interface remains challenging to sensorize. We want wearable robots to dynamically respond to changes in both the external environment and human output. This dynamic response requires real-time feedback of the mechanical interactions between the user and their machine. However, current approaches mostly instrument solely the human *or* the robot, limiting our understanding of the state of the complete system [4]. Current human-centered metrics like electromyography (EMG) and metabolic energy consumption often have low signal to noise ratios (SNRs) and slowly changing dynamics [5], making it challenging for robot controllers to adapt to user behavior in real time. Robot-centered metrics like inertial measurement units (IMUs), reaction torque sensors, motor-generated voltages, and Bowden cable lengths measure the human by proxy [6, 7], which can introduce delays and uncertainty between the real and measured signals. This complicates real-time control, as evidenced by recent efforts that use machine learning to combine multiple proxy measurements to achieve gait assistance [8, 9].

Previous systems have measured human-robot interaction forces by adding force sensors into pads, straps and other mechanical attachments within the robot body. Force-sensitive resistors (FSRs) are the most popular sensors due to their

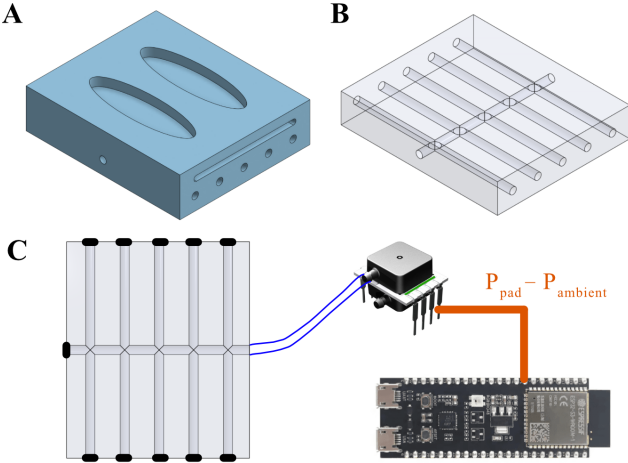


Fig. 2. CAD render and system overview of the fluidically innervated pad. (A) Render of the entire pad with upper slot for strap attachment. (B) Transparent view without the strap slot showing interconnected channel structure yielding one bulk pressure reading. (C) Schematic of connection to readout electronics. All openings are sealed (black) except one connected via tubing (blue) to a differential pressure transducer measuring pad pressure relative to ambient air, with data recorded by a microcontroller.

low cost and straightforward electronics [10, 11]. However, their non-linear response curve and significant imprecision limit their utility in applications requiring fast and accurate readings [12]–[14]. Optoelectric and pneumatic solutions offer higher accuracy, but at the cost of multi-step casting for fabrication [15]–[17]. 3D printing offers a potential way to ease fabrication difficulties, but current capacitive-based solutions require fine measurements of small capacitance changes [18]. A sensing solution that is simple to manufacture, has high time resolution, and is adaptable across human interfaces has the potential to facilitate more robust real-time and dynamic control of wearable robotics.

In this work, we introduce fluidic innervation as a promising method for mechanical sensing of human-machine interaction in wearable devices (Fig. 1). Fluidic innervation is a sensorization technique that adds force sensing to any 3D printed structure by embedding internal channels filled with air at ambient pressure within the structure [19]. Compression of the structure therefore compresses the internal air channels, producing changes in pressure measurable by off-the-shelf transducers. Because fluidic innervation leverages 3D printed soft material with off-the-shelf portable components, application-specific designs can be rapidly fabricated. Fluidic innervation has been demonstrated to have a high SNR and time resolution in soft robotic grippers [20, 21]. However, this technique has not yet been applied to sensorize the human-robot interface in wearable systems, which innately have more variability than robotic applications.

First, we demonstrate the design of fluidic innervated pads that can be worn on a human limb. Next, we characterize performance through off-human mechanical compression testing and on-human testing during isometric torque generation with a clinical dynamometer. Finally, we demonstrate the pads in less constrained tasks, including isometric and dynamic bicep curls as well as squats. Our results validate

fluidic innervation-based sensing of human–machine interaction across multiple activities, motivating future measurement of human-device behavior and potential use as a control input in actuated robotic devices.

II. METHODS

To adapt fluidic innervation to the human context, we designed a soft, comfortable pad that can easily be placed on the human body while minimally interfering with movement. There are 3 major components to the wearable system: the fluidically innervated pad, readout electronics, and attachment to the human body (Fig. 1C). The pad design and readout electronics were adapted from our prior work developing sensorized robots [19, 21].

Each sensorized pad ($75 \times 64 \times 14$ mm) was designed with an internal air channel embedded within the structure to provide pressure sensing information (Fig. 2A–B). Because we are interested in bulk force metrics as an initial testbed, we designed the pad’s internal channel structure to be a series of interconnected channels, forming a single cavity that covers most of the pad area. This differs from our prior research where a single structure contained multiple channels, but future pad designs of multiple channels to extract finer resolution surface force distributions are feasible.

Each pad was fabricated by a resin 3D printer using Silicone 40 (Formlabs). This material was chosen because it is one of the softest commercial resins available, promoting maximum comfort. After printing, each channel (3.2 mm in diameter) was flushed with solvent and compressed air to ensure it was empty before sealing all but one end. This open end was connected to an off-the-shelf pressure transducer (AllSensors 10 in. H_2O) to measure the pressure within the channels of the pad (Fig. 2C). Channel ends were sealed with Sil-poxy and cyanoacrylate glue, while the open channel end was connected to the pressure transducer via silicone tubing with plastic barbs. We used differential pressure transducers, but compare the measured pressure to ambient air (i.e., one port disconnected). This setup means that if the channels were bent but not compressed, the channel’s volume of air would increase and a “negative” pressure would be reported [19]. The pressure transducer voltage was read via I2C by an ESP32, which then communicated via Bluetooth to a computer for data recording (sampled at 50 Hz).

For consistency, we used the same pad for all experiments. However, 3D printing makes it easy to change pad dimensions for a better fit to a specific person. Here, we showcase this customization by printing the pads with various “slot” geometries to accommodate different straps for each application while the channel layout within each pad remained the same. Three different strap attachments were used for our in-human applications: clinical dynamometer (Sec. III-B), bicep curls (Sec. IV-A), and squats (Sec. IV-B). This fabrication flexibility demonstrates adaptability to capture human machine interaction and is possible due to fluidic innervation’s foundation on 3D printing.

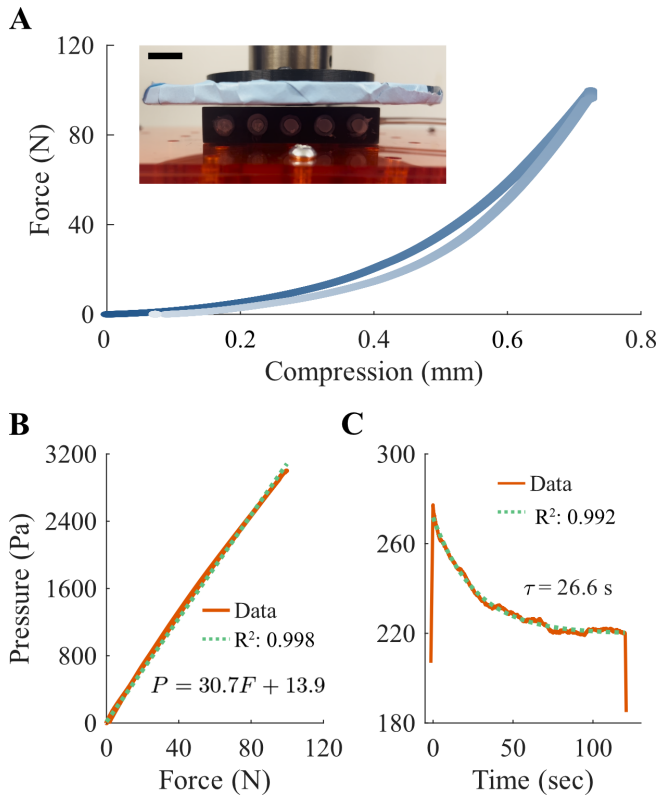


Fig. 3. Characterization of sensorized pad using mechanical testing machine. (A) Mean compression distance vs. force across three trials. The maximum standard deviation was 0.15 N and $< 10^{-2}$ mm (not visible). The inset shows the compression test setup (scale bar 1 cm). (B) Mean force vs. sensorized pad pressure was highly linear ($R^2: 0.998$, maximum standard deviation 32 Pa, not visible). (C) Exemplar trial in which the pad was compressed until 20 N, after which the position was held for 2 minutes. Stress relaxation in pressure readings were observed due to viscoelastic material properties, with an exponential decay time constant τ of 26.6 s.

III. CHARACTERIZATION

A. Off-board Mechanical Testing

The pads' ability to accurately measure applied force was validated on a mechanical testing machine (Shimadzu AGS-X). Each pad was placed under a compression plate to measure performance under bulk deformation. The mechanical testing machine provided ground truth of applied force for a given compression amount (Fig. 3A). We downsampled and interpolated the 100 Hz data to match the sensorized pad's 50 Hz rate, and correlated force with pad pressure (Fig. 3B).

A preliminary compression test determined the force at which the pressure transducer saturated. Although rated for 2490 Pa, we found a measurement limit of 3114 Pa at 113 N. Thus, we conducted compression trials between 0 – 100 N. We compressed the pad at 1 mm/s up to 100 N, held position for 10 s and unloaded at the same rate. We performed three trials and reported mean and maximum standard deviation.

Sensorized pad pressure was highly linearly correlated with ground truth force (Fig. 3B, $P = 30.7F + 13.9$, $R^2 = 0.998$). This linear relationship existed despite the non-linearity and hysteresis of the force vs. compression test (Fig. 3A), which was expected because of silicone's viscoelastic properties. The tight correlation between force

and pressure indicates the sensorized pad does not add *additional* non-linearity to the system, constituting a significant improvement over traditional approaches like FSRs, which suffer from inaccuracy due to their non-linearity [12].

Consistent with previously observed results of fluidically innervated sensors [19], we observed a significant amount of stress relaxation during the hold period of the compression tests. Because this decay response affects pressure readings, we quantified it during a long step compression test wherein the pad was compressed until 20 N of force was measured and then the position of the compression plate was held for two minutes before unloading the pad (Fig. 3C). We fit an exponential decay curve to this response, yielding a time constant of $\tau = 26.6$ s. The wearable pads are intended to capture forces during human movements lasting 2-3 seconds at most, indicating this decay will have minimal effect. Overall, these results demonstrate fluidic innervated pads accurately measure applied forces, making them a good fit to measure human-machine interaction.

B. On-Human Testing with Clinical Dynamometer

To demonstrate feasibility of fluidic innervation to capture user-device interaction, we constructed a benchtop setting, where a pad was mounted on a human limb while the person performed a well-controlled simple task. A single healthy individual (male, age 42 years) produced volitional isometric knee torque while seated in a clinical dynamometer (Biodex System 4 Pro) with their knee fixed at 45° (Fig. 4). Four conditions were tested involving two pad locations (above and below knee (Fig. 4B,E)) and two torque directions (knee extension and flexion). The experiment order was conducted with the pad above the knee followed by below the knee, and within each location, extension followed by flexion. Within each condition, four trials were completed, with 5 s of rest, 5 s holding torque at 10 N m, and another 5 s of rest (Fig. 4A). The user was provided real time feedback of their torque output. Dynamometer torque and pad pressure were acquired as synchronized analog inputs (National Instruments USB-6211, sample rate 1000 Hz) into MATLAB (Mathworks, Natick, MA). After the experiment, torque and pressure data were converted from V to N m and Pa, respectively. Data were offset by the mean during the initial rest from 0.5 to 2 s to compute relative changes during the activity, and lowpass filtered to isolate task dynamics (6 Hz cutoff). Torque and pad data across all trials for each condition were linearly correlated, and R^2 values for the model were extracted.

The user successfully modulated torque and held a steady-state value of approximately 10 N m. Strikingly, pad pressure yielded both a very high signal to noise ratio from rest to 10 N m and a very fast signal response to changes in volitional torque (Fig. 4A) in the scenario with the clearest interaction between pressure and torque output (pad above the knee during flexion as in Fig. 4B). Linear fits between torque and pad pressure varied by location and torque direction. Notably, the pad above the knee (Fig. 4B) more accurately captured knee flexion (Fig. 4C) with a maximum measurement of approximately 200 Pa ($R^2 = 0.95$). Meanwhile, the pad below

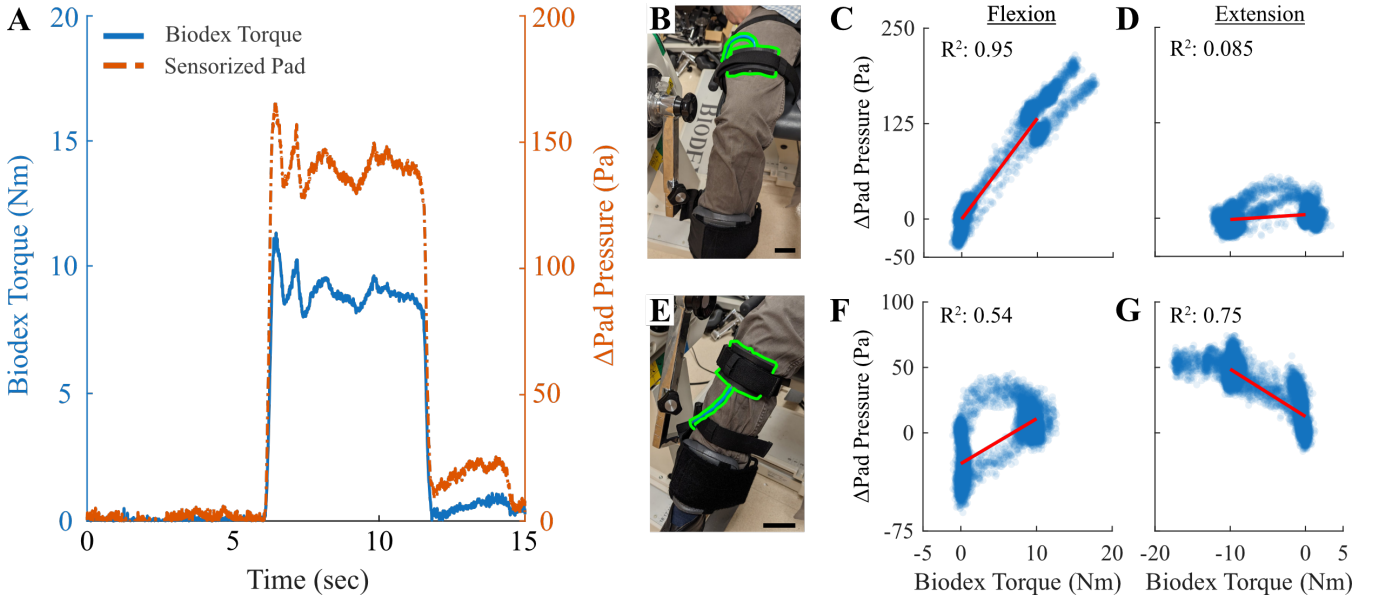


Fig. 4. Characterization of sensorized pads through on-human dynamometer testing. Participants repeated isometric volitional knee torque output to 10 Nm while dynamometer torque and pad pressure were recorded simultaneously. (A) Exemplary time series data from knee flexion with (B) the fluidically innervated pad above the knee. (C-D) Correlation results between the measured pressure of the above-knee pad and the measured dynamometer torque during flexion and extension. (E) Tests were also performed with the fluidically innervated pad below the knee. (F-G) Correlation results between the measured pressure of the below-knee pad and the measured dynamometer torque during flexion and extension. Scale bars represent 5 cm.

the knee (Fig. 4E) more accurately captured knee extension (Fig. 4G) with a range of 60 Pa, $R^2 = 0.75$. In contrast, extension above the knee (Fig. 4D) and flexion below the knee (Fig. 4F) yielded weak relationships ($R^2 = 0.085$ and 0.54, respectively). This was not surprising because the force applied by the shank during extension pushed into the pad, whereas in flexion, the force pushes away. Conversely, during extension, the thigh applied forces downward into the seat, which the pad would not register as accurately; however, in flexion, the thigh applies forces into the pad with measurable deformation. Additionally, the pad below the knee was adjacent to the dynamometer mount on the same segment, thus registering only a portion of segment loading and likely distorting the measured pressure signal. Future studies should integrate fluidically innervated pads directly at the dynamometer mount or primary human-machine interaction site to eliminate the confounding effect of pad placement. Nonetheless, these results suggest strategic pad design can capture user-device interactions with high fidelity.

IV. RESULTS

To evaluate fluidic innervation's capture of human-device interaction during unconstrained movement, we present two test cases featuring cyclic motion of upper- and lower-limbs.

A. Dynamic and Isometric Bicep Curl Experiment

For the upper-limb experiments, the sensing pad was mounted on the *biceps brachii* of a single healthy individual (female, 30 years) by feeding a strap through the pad (Fig. 1C). Elbow flexion was first repeated from 90° to full flexion and then returning back to 90° five times (cycle time 4 s) while holding no weight, as well as holding a mass of 0.5, 1, 2.27, and 4.54 kg in her hand. Thereafter, for each

mass, the user conducted another 5 cycles, where within each cycle, they paused at $\approx 120^\circ$, 135° , and 150° for 4 s each. For the dataset with full cycles, pressure data were filtered and offset, each cycle was normalized (linear interpolation, 100 data points), and the mean and standard deviation across cycles were computed for each mass (Fig. 5). In the stepwise cycles, to extract steady-state pressure at each position, a 2 s region with the lowest coefficient of variation within each cycle was isolated and averaged (Fig. 6A). A 2-way analysis of variance assessed effects of elbow angle, mass held, and their interaction, with post-hoc multiple comparisons conducted for any significant effects (Tukey's LSD).

In the dynamic full cycles of elbow flexion (Fig. 5), the pad pressure exhibited a clear correlation between pressure and elbow angle across all masses. Pressure sharply increased then decreased with remarkable repeatability across cycles. Unexpectedly, non-monotonic peak pad pressure was observed with increases in the mass held in the hand. Highest peak pressure of 2000 Pa was seen with no load, followed by 1200 Pa with 1 kg, and lower peak pressures ranging between 600 to 800 Pa for 0.5, 2.27, and 4.45 kg.

These trends persisted in the stepwise isometric bicep curls (Fig. 6). Elbow angle strongly influenced pad pressure across all loads ($F(2, 60) = 772.5$, $p < 0.001$), with pressure increasing with flexion. There was a significant effect of load ($F(4, 60) = 103.8$, $p < 0.001$) where a general reduction in pressure was observed for increasing mass at each angle; however this was not strictly monotonic as pressures in 0.5 kg were significantly lower than 0 and 1 kg but significantly greater than 2.27 and 4.54 kg. A significant angle-load interaction was present ($F(8, 60) = 2.87$, $p = 0.009$), with more flexion tending to amplify pressure differences at

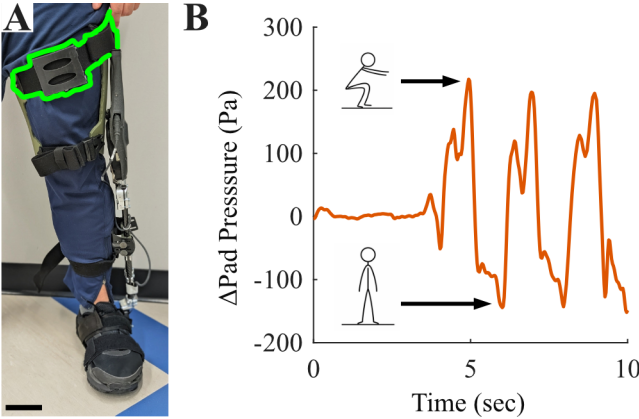


Fig. 7. (A) Fluidically innervated pads were integrated into a robotic exoskeleton [22]. Scale bar is 5 cm. (B) Relative change in pad pressure followed the dynamics squats (2 s cycle time, three of ten shown for brevity).

IMU or other sensors may lead to improved interpretation of pressure readings in terms of human effort by accounting for limb dynamics. Second, it is likely that simultaneous deployment of multiple pressure pads, or distinct pressure sensing channels within a larger surface area, would enhance characterization of the human-machine interface.

Nevertheless, our initial results show promise for integration of sensorized pads to accurately quantify interaction force in wearable robotic applications with high resolution and low latency. In the future this high-fidelity measurement could provide useful information during device use, such as user movement intent and force output, which could be directly integrated into the control loop to adapt and optimize robotically applied forces in real time [23] and over longer time scales [5]. Direct force measurement could also enhance user comfort by enabling real-time minimization of interaction forces as well as providing valuable information on pressure distributions to inform future device designs.

ACKNOWLEDGMENT

This research was supported by the Intramural Research Program at the National Institutes of Health (NIH), the Texas Robotics Industrial Affiliates Program, and the Schmidt Science Fellows program. The contributions of the NIH authors are considered Works of the United States Government. The findings and conclusions presented in this paper are those of the authors and do not necessarily reflect the views of the NIH or the U.S. Department of Health and Human Services.

REFERENCES

- [1] J. Rosen, *Wearable Robotics: Systems and Applications*. Academic Press, Nov. 2019.
- [2] M. Zhu, S. Biswas, S. I. Dinulescu, N. Kastor, E. W. Hawkes, and Y. Visell, "Soft, Wearable Robotics and Haptics: Technologies, Trends, and Emerging Applications," *Proceedings of the IEEE*, vol. 110, pp. 246–272, Feb. 2022.
- [3] P. G. Adamczyk, S. E. Harper, A. J. Reiter, R. A. Roembke, Y. Wang, K. M. Nichols, and D. G. Thelen, "Wearable sensing for understanding and influencing human movement in ecological contexts," *Current opinion in biomedical engineering*, vol. 28, p. 100492, 2023.
- [4] J. Babić, M. Laffranchi, F. Tessari, T. Verstraten, D. Novak, N. Šarabon, B. Uğurlu, L. Peternel, D. Torricelli, and J. F. Veneman, "Challenges and solutions for application and wider adoption of wearable robots," *Wearable Technologies*, vol. 2, p. e14, Jan. 2021.
- [5] J. Zhang, P. Fiers, K. A. Witte, R. W. Jackson, K. L. Poggensee, C. G. Atkeson, and S. H. Collins, "Human-in-the-loop optimization of exoskeleton assistance during walking," *Science*, vol. 356, no. 6344, pp. 1280–1284, 2017.
- [6] S. Lee, S. Crea, P. Malcolm, I. Galiana, A. Asbeck, and C. Walsh, "Controlling negative and positive power at the ankle with a soft exosuit," in *2016 IEEE International Conference on Robotics and Automation (ICRA)*, pp. 3509–3515, May 2016.
- [7] L. Lunenburger, G. Colombo, R. Riener, and V. Dietz, "Biofeedback in gait training with the robotic orthosis Lokomat," in *The 26th Annual International Conference of the IEEE Engineering in Medicine and Biology Society*, vol. 2, pp. 4888–4891, Sept. 2004.
- [8] D. D. Molinaro, K. L. Scherpereel, E. B. Schonhaut, G. Evangelopoulos, M. K. Shepherd, and A. J. Young, "Task-agnostic exoskeleton control via biological joint moment estimation," *Nature*, vol. 635, pp. 337–344, Nov. 2024.
- [9] S. Luo, M. Jiang, S. Zhang, J. Zhu, S. Yu, I. Dominguez Silva, T. Wang, E. Rouse, B. Zhou, H. Yuk, X. Zhou, and H. Su, "Experiment-free exoskeleton assistance via learning in simulation," *Nature*, vol. 630, pp. 353–359, June 2024.
- [10] J. Tamez-Duque, R. Cobian-Ugalde, A. Kilicarslan, A. Venkatakrishnan, R. Soto, and J. L. Contreras-Vidal, "Real-time strap pressure sensor system for powered exoskeletons," *Sensors*, vol. 15, no. 2, pp. 4550–4563, 2015.
- [11] J. Bessler, L. Schaake, R. Kelder, J. H. Buirke, and G. B. Prange-Lasonder, "Prototype measuring device for assessing interaction forces between human limbs and rehabilitation robots-a proof of concept study," in *2019 IEEE 16th International Conference on Rehabilitation Robotics (ICORR)*, pp. 1109–1114, IEEE, 2019.
- [12] E. I. G. Velásquez, V. Gómez, L. Paredes-Madrid, and H. A. Colorado, "Error compensation in force sensing resistors," *Sensing and Bio-Sensing Research*, vol. 26, p. 100300, 2019.
- [13] H. Choi, K. Seo, S. Hyung, Y. Shim, and S.-C. Lim, "Compact hip-force sensor for a gait-assistance exoskeleton system," *Sensors*, vol. 18, no. 2, p. 566, 2018.
- [14] A. Rathore, M. Wilcox, D. Z. M. Ramirez, R. Loureiro, and T. Carlson, "Quantifying the human-robot interaction forces between a lower limb exoskeleton and healthy users," in *2016 38th Annual International Conference of the IEEE Engineering in Medicine and Biology Society (EMBC)*, pp. 586–589, IEEE, 2016.
- [15] T. Lenzi, N. Vitiello, S. M. M. De Rossi, A. Persichetti, F. Giovacchini, S. Roccella, F. Vecchi, and M. C. Carrozza, "Measuring human–robot interaction on wearable robots: A distributed approach," *Mechatronics*, vol. 21, no. 6, pp. 1123–1131, 2011.
- [16] K. Langlois, D. Rodriguez-Cianca, B. Serrien, J. De Winter, T. Verstraten, C. Rodriguez-Guerrero, B. Vanderborght, and D. Lefebvre, "Investigating the effects of strapping pressure on human-robot interface dynamics using a soft robotic cuff," *IEEE transactions on Medical Robotics and Bionics*, vol. 3, no. 1, pp. 146–155, 2020.
- [17] S. Wang, B. Zhang, Z. Yu, and Y. Yan, "Differential soft sensor-based measurement of interactive force and assistive torque for a robotic hip exoskeleton," *Sensors*, vol. 21, no. 19, p. 6545, 2021.
- [18] K. Langlois, E. Roels, G. Van De Velde, C. Espadinha, C. Van Vlerken, T. Verstraten, B. Vanderborght, and D. Lefebvre, "Integration of 3d printed flexible pressure sensors into physical interfaces for wearable robots," *Sensors*, vol. 21, no. 6, p. 2157, 2021.
- [19] R. L. Truby, L. Chin, A. Zhang, and D. Rus, "Fluidic innervation sensorizes structures from a single build material," *Science advances*, vol. 8, no. 31, p. eabq4385, 2022.
- [20] A. Zhang, L. Chin, D. L. Tong, and D. Rus, "Embedded air channels transform soft lattices into sensorized grippers," in *2024 IEEE International Conference on Robotics and Automation (ICRA)*, pp. 5264–5270, IEEE, 2024.
- [21] S. Shang, M. Seo, Y. Zhu, and L. Chin, "Forte: Tactile force and slip sensing on compliant fingers for delicate manipulation," *arXiv preprint arXiv:2506.18960*, 2025.
- [22] T. M. Devine, A. Asante-Otoo, K. Alter, D. L. Damiano, and T. C. Bulea, "Robotic knee exoskeletons as assistive and gait training tools in spina bifida: A pilot study showing clinical feasibility of two control strategies," *IEEE Transactions on Neural Systems and Rehabilitation Engineering*, 2025.
- [23] N. V. Divekar, G. C. Thomas, A. R. Yerva, H. B. Frame, and R. D. Gregg, "A versatile knee exoskeleton mitigates quadriceps fatigue in lifting, lowering, and carrying tasks," *Science Robotics*, vol. 9, no. 94, p. eadr8282, 2024.